

## ***Seasonal Climate Variability and Change in the Pacific Northwest of the United States***

The Faculty of Oregon State University has made this article openly available.  
Please share how this access benefits you. Your story matters.

<b>Citation</b>	Abatzoglou, J. T., Rupp, D. E., & Mote, P. W. (2014). Seasonal climate variability and change in the Pacific Northwest of the United States. <i>Journal of Climate</i> , 27 (5), 2125-2142. doi:10.1175/JCLI-D-13-00218.1
<b>DOI</b>	10.1175/JCLI-D-13-00218.1
<b>Publisher</b>	American Meteorological Society
<b>Version</b>	Version of Record
<b>Terms of Use</b>	<a href="http://cdss.library.oregonstate.edu/sa-termsfuse">http://cdss.library.oregonstate.edu/sa-termsfuse</a>

# Seasonal Climate Variability and Change in the Pacific Northwest of the United States

JOHN T. ABATZOGLOU

*Department of Geography, University of Idaho, Moscow, Idaho*

DAVID E. RUPP AND PHILIP W. MOTE

*Oregon Climate Change Research Institute, Oregon State University, Corvallis, Oregon*

(Manuscript received 12 April 2013, in final form 31 October 2013)

## ABSTRACT

Observed changes in climate of the U.S. Pacific Northwest since the early twentieth century were examined using four different datasets. Annual mean temperature increased by approximately 0.6°–0.8°C from 1901 to 2012, with corroborating indicators including a lengthened freeze-free season, increased temperature of the coldest night of the year, and increased growing-season potential evapotranspiration. Seasonal temperature trends over shorter time scales (<50 yr) were variable. Despite increased warming rates in most seasons over the last half century, nonsignificant cooling was observed during spring from 1980 to 2012. Observations show a long-term increase in spring precipitation; however, decreased summer and autumn precipitation and increased potential evapotranspiration have resulted in larger climatic water deficits over the past four decades. A bootstrapped multiple linear regression model was used to better resolve the temporal heterogeneity of seasonal temperature and precipitation trends and to apportion trends to internal climate variability, solar variability, volcanic aerosols, and anthropogenic forcing. The El Niño–Southern Oscillation and the Pacific–North American pattern were the primary modulators of seasonal temperature trends on multidecadal time scales: solar and volcanic forcing were nonsignificant predictors and contributed weakly to observed trends. Anthropogenic forcing was a significant predictor of, and the leading contributor to, long-term warming; natural factors alone fail to explain the observed warming. Conversely, poor model skill for seasonal precipitation suggests that other factors need to be considered to understand the sources of seasonal precipitation trends.

## 1. Introduction

A variety of lines of evidence support the conclusions that global mean surface temperature has increased during the past half century and that anthropogenic drivers are largely responsible for the warming (Trenberth et al. 2007; Alexander et al. 2013). Global mean surface temperature is the most widely cited indicator of climate change and is directly tied to changes in the global energy budget. However, local-to-regional changes in temperature are more varied owing to regional influences of internal climate variability (e.g., Deser et al. 2012; Pierce et al. 2008). As climate impacts are manifested at local and regional scales, it is important to

discern between natural or unforced variability and anthropogenic forcing. Likewise, a thorough understanding of apportioning these factors is vital for framing regional climate projections in the context of natural variability.

Observed changes in regional temperature are generally a result of internal climate variability and anthropogenic radiative change, with the drivers playing complementary or competing roles (e.g., Wallace et al. 2012). Internal climate variability as manifested through preferred modes of atmospheric circulation and decadal sea surface temperature variability have modulated temperature trends globally (e.g., Thompson et al. 2009; Foster and Rahmstorf 2011) and regionally, including western North America during the cool season (e.g., Wang et al. 2009; Abatzoglou and Redmond 2007; Abatzoglou 2011). Internal climate variability will continue to modify the pace of regional climate change, potentially obscuring anthropogenic-forced regional change for the next several

---

*Corresponding author address:* Dr. John T. Abatzoglou, Department of Geography, 875 Perimeter Dr., MS 3021, Moscow, ID 83844-3021.

E-mail: jabatoglou@uidaho.edu

decades (e.g., Deser et al. 2012) and is a significant source of uncertainty for near-term regional climate projections (Hawkins and Sutton 2011).

Although mean annual temperature is the most cited global indicator of climate change, seasonal temperature and precipitation at regional scales provide more salient links to climate impacts that may be otherwise masked in mean annual temperature. A prime example pertaining to the Pacific Northwest (PNW) of the United States is the influence of winter and spring temperature to a suite of hydrologic impacts in snowmelt-driven watersheds (e.g., Mote et al. 2005). Likewise, teleconnections associated with internal climate variability have distinct seasonal controls on regional climate that contribute to climate impacts. Biophysically and socially relevant climate derivatives, including the length of the freeze-free season, annual temperature extremes, and growing-season potential evapotranspiration, all of which can be linked to seasonal climate, often provide a more direct link to climate impacts than annual or seasonal temperature and precipitation and are readily accessible climate information for scientific communication (e.g., Betts 2011).

Formal attribution of regional climate change remains more challenging owing to the regional manifestation of internal climate variability, aerosols, and land surface interactions (e.g., Stott et al. 2010; Deser et al. 2012). Bonfils et al. (2008) showed that late winter–early spring trends in temperature and hydrologically relevant temperature metrics over the western United States were attributable to net anthropogenic forcings rather than natural variability (i.e., internal climate variability and solar and volcanic variability). A simpler approach of filtering out the influences of natural climate variability is through the use of multiple linear regression (MLR). Lean and Rind (2008) used MLR of El Niño–Southern Oscillation (ENSO), solar activity, and volcanic and anthropogenic influences to explain spatial patterns of annual mean surface temperature change. They showed that a linear combination of these four factors accounted for over three-quarters of the variance of global mean annual surface temperature from 1889 to 2006 and, moreover, that warming due to anthropogenic forcing was an order of magnitude greater than net warming due to the remaining factors. Foster and Rahmstorf (2011) applied a similar approach to linearly disaggregate natural influences on global averaged surface and lower-tropospheric annual temperature since 1979. They showed that removing the estimated linear effects of solar, volcanic, and ENSO variability better isolated the signal of planetary warming and elucidated a warming signal on shorter time scales ( $\sim 30$  yr) that was otherwise masked by the combination of nonanthropogenic factors.

Mote (2003) showed that temperatures in the PNW increased  $0.7^{\circ}$ – $0.9^{\circ}\text{C}$  during the twentieth century and that precipitation increased primarily during spring and summer. He showed that roughly 30% of the warming during winter from 1920 to 2000 could be explained by internal climate variability represented by the North Pacific index. Although no explicit attempt was made to identify the causal connection to anthropogenic radiative forcing, Mote and Salathé (2010) examined 20 Coupled Model Intercomparison Project phase 3 (CMIP3) climate model simulations of the twentieth century driven by observed greenhouse gas concentrations and found that most models simulated regional temperature trends consistent with observations.

In this paper, we update and improve upon the work of Mote (2003) by examining observed seasonal trends in temperature and precipitation for the PNW, in addition to a set of biophysically and socially relevant metrics across a variety of time scales. Moreover, we extend the methods of Lean and Rind (2008) and Foster and Rahmstorf (2011) to regional and seasonal scales in order to better understand the sources of observed temperature and precipitation trends in the PNW and the extent to which they can be explained through natural variability and anthropogenic forcing. Improved comprehension of factors responsible for seasonal temperature trends may help resolve the asymmetry of observed seasonal trends and their manifestation on mean annual temperature trends (e.g., Cohen et al. 2012).

## 2. Data and methods

The PNW is defined here as encompassing the landmass of the contiguous United States north of  $42^{\circ}\text{N}$  west of  $110^{\circ}\text{W}$ , comprising the states of Oregon, Washington, and Idaho as well as western Montana and extreme northwestern Wyoming. We used four observational datasets to better assess uncertainty of changes in the observational record: (i) daily and monthly maximum and minimum temperature and precipitation from 141 stations in the U.S. Historical Climate Network, version 2.5 (USHCN v2.5) (Menne et al. 2009); (ii) gridded monthly temperature and precipitation from the Parameter-Elevation Regressions on Independent Slopes Model (PRISM) (Daly et al. 2008); (iii) gridded monthly temperature and precipitation data from Climatic Research Unit (CRU) TS3.21 dataset (Harris et al. 2013); and (iv) monthly temperature from the U. S. climate division dataset from the National Climatic Data Center (NCDC) and monthly precipitation from the U.S. climate division dataset adjusted for inhomogeneities (McRoberts and Nielsen-Gammon 2011). The latter three datasets were considered for the time period 1901–2012.

Although station observations extend back prior to 1920, Mote (2003) showed that the number of reporting USHCN stations increased from a few before 1900 to a near complete set by 1925. We therefore restricted our station analysis to the period 1920–2012. Months with more than five missing days were considered “missing,” as were seasons or years with any missing months. Monthly temperature data for the USHCN v2.5 are subjected to a series of checks designed to remove nonclimatic effects on each station’s temperature time series, including climate inhomogeneities (e.g., changes in observational methods and/or location) and urbanization. Estimates are also made for missing data using neighboring station observations. No adjustments for climate inhomogeneities are made for precipitation or for daily data. Prior studies have shown that subregional-scale (<100 km) changes in climate can be a response to land-use changes and dynamical processes and may be of different magnitudes and direction compared to regional-scale changes in the presence of complex topography. Thus, we examined trends at individual stations to contextualize regional trends, as the primary focus of this study is on regional-scale (~1000 km) changes in climate, rather than the details of localized change.

Time series of monthly regional temperature and precipitation from PRISM and CRU were constructed by taking the areal mean of gridded data (30-arc-s horizontal resolution for PRISM, and 0.5° resolution for CRU). Regional averaged data from NCDC divisional data were constructed using area-weighted polygons of all climate divisions in Washington, Oregon, and Idaho and climate division 1 and 2 in Montana. These datasets are not independent, but rather all draw on different combinations of station observations in aggregating to coarser scales, different methods to adjust for nonclimatic changes in station data, and different quality control procedures. Rather than relying on a single regional dataset, we considered the structural uncertainty inherent with dataset development (e.g., Morice et al. 2012) to resolve the sensitivity of our results to the choice of observational dataset. We considered trends in calendar year mean temperature, water year cumulative precipitation, and standard climatological seasons of winter [December–February (DJF)], spring [March–May (MAM)], summer [June–August (JJA)], and fall [September–November (SON)].

We considered several additional metrics to supplement the analysis of seasonal temperature and precipitation: (i) the last date in spring (March–June) and first date in autumn (July–November) with daily minimum temperatures below 0°C, that is, the length of the freeze-free season (number of days between the last

spring freeze and first autumn freeze), (ii) the absolute minimum temperature each winter (November–March) and absolute maximum temperature each summer (June–September), (iii) growing-season (freeze free) reference evapotranspiration (ET<sub>o</sub>), and (iv) annual climatic water deficit. For all metrics, stations missing more than 20% of observations during a given recording period were excluded.

Daily ET<sub>o</sub> was estimated using the Penman–Montieth equation (Allen et al. 1998), climatological downward shortwave radiation and wind speeds from phase 2 of the North American Land Data Assimilation System (NLDAS-2) (Mitchell et al. 2004), and retrospective temperature and estimated vapor pressure deficit from USHCN observations. Daily mean dewpoint temperature was estimated by subtracting monthly mean dewpoint depression (minimum temperature minus dewpoint temperature) bilinearly interpolated from PRISM from observed daily minimum temperature for each station. Daily vapor pressure deficit was then estimated from mean dewpoint temperature and daily maximum and minimum temperature following Jensen et al. (1990). Daily ET<sub>o</sub> was set to 0 outside of the freeze-free season to account for reduced water demand and reduced transpiration during the cool season. A modified Thornthwaite water balance model (Willmott et al. 1985; updated by Dobrowski et al. 2013) that incorporates monthly temperature, precipitation, and ET<sub>o</sub> was run at monthly time steps with standard 150-mm soil water holding capacity to model monthly climate water deficit. We define climatic water deficit as unmet atmospheric demand, or the difference between ET<sub>o</sub> and actual evapotranspiration for a reference crop.

Trends were computed using a linear least squares regression for datasets that had complete data for at least 75% of each time period considered. Statistical significance ( $p < 0.05$ ) was determined by computing the standard error of the trend estimate, where temporal autocorrelation is taken into account by adjusting the degrees of freedom (Santer et al. 2000). Trend analyses often represent a trade-off between long-term data with sparse spatial coverage or more complete spatial coverage over limited durations (e.g., Liebmann et al. 2010). To investigate the suitability of linear fits in depicting observed changes, linear trends were computed using varying starting years of 1901 and staggered every 10 years from 1910 to 1980, with the ending year defined by the last year of observations (2012).

We followed the general approach of Lean and Rind (2008, 2009) and Foster and Rahmstorf (2011) in performing MLR for regional seasonal temperature and precipitation by considering five forcing factors: (i) ENSO, (ii) the Pacific–North American (PNA) pattern, (iii) solar

variability, (iv) volcanic aerosols, and (v) anthropogenic radiative forcing. Details of the datasets used to represent these factors are provided in the appendix.

We performed MLR analysis separately for each season, recognizing that the balance of factors may change with the seasons. Only concurrent relationships between seasonal forcings and temperature were examined. We chose this approach over optimizing lag relationships as done in Lean and Rind (2008) and Foster and Rahmstorf (2011) with global mean temperature, given the potential problems of overfitting and challenges in dynamically explaining lag responses to these forcings. Multiple linear regression is best suited for orthogonal predictors, such as with principal component analysis; however, the predictors in this study were not orthogonal, particularly PNA and ENSO. To avoid problems resulting from collinearity of PNA with ENSO, we used the partial correlation of PNA for a fixed multivariate El Niño index (MEI). This was accomplished by subtracting a linear regression of MEI to the PNA from the PNA index, resulting in a residual PNA (PNAr) that is uncorrelated to MEI. We used the PNAr and the MEI, rather than vice versa, given the well-documented dynamical links between the boundary forcing of tropical SST forcing associated with ENSO and PNA phase (e.g., Horel and Wallace 1981). Altering the order of operations by using the raw PNA and a residual MEI (uncorrelated to PNA) had no net influence of the combined modes of natural variability on our study, although it resulted in stronger relationships to PNA and weaker relationships to the residual MEI. However, collinearity between other predictors was still present and is discussed further.

A bootstrapping procedure with replacement was used to increase the robustness of modeled relationships and to compute confidence intervals for our relationships. The MLR was run 1000 times by randomly selecting 112 years with replacement yielding 1000 different model realizations for each season. We calculated residuals of the observed time series minus the MLR as well as residuals of the observed time series minus the MLR where the coefficients for anthropogenic forcing were set to 0. This analysis was done separately for the three regional datasets. Results are reported by pooling the MLR results; however, significant differences in MLR between datasets are noted.

### 3. Results

#### a. Regional averages

Regional annual mean temperature (Fig. 1a) shows long-term warming modulated by interdecadal variability with

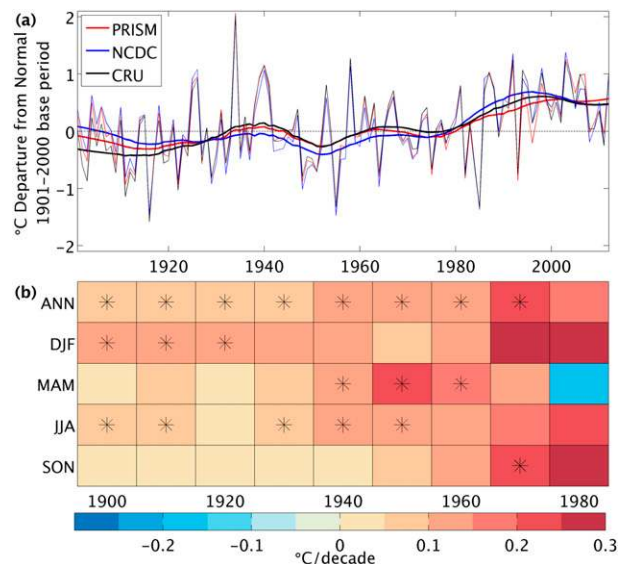


FIG. 1. (a) Annual mean, regional mean temperature anomaly for PRISM (red), NCDC divisional data (blue), and CRU (black) from 1901 to 2012. Anomalies are taken with respect to the 1901–2000 period. Bold lines show a local weighted regression. (b) Linear least squares trend in regional mean temperature ( $^{\circ}\text{C decade}^{-1}$ ) averaged over the calendar year and for each season for the time interval beginning with the year on the bottom axis through 2012. An average of the anomalies computed for the three different datasets is used in (a). Statistically significance ( $p < 0.05$ ) is denoted by asterisks.

relatively cool periods 1910–25 and 1945–60 and relatively warm periods around 1940 and since the mid-1980s. The warmest year in the region was 1934, but the warmest 10-yr period was 1998–2007, with very few years since 1980 that had below-average annual mean temperatures. Linear trends in annual mean temperature from 1901 to 2012 were between  $0.056^{\circ}$  and  $0.076^{\circ}\text{C decade}^{-1}$ , with larger warming found in the CRU dataset. Differences among the three regional datasets were largest (but still small) prior to 1920 when the number of station observations was most limiting. The CRU data were cooler than PRISM and NCDC over the 1900–30 time period and, hence, had a larger long-term warming trend over the period of record, particularly for the first half of the twentieth century; however, linear trends estimated from the different datasets varied by less than 30% generally. Observations show an accelerated warming rate with linear trends for the 1970–2012 and 1980–2012 time periods of approximately  $0.2^{\circ}\text{C decade}^{-1}$  (Fig. 1b), similar to that seen globally (e.g., Trenberth et al. 2007, p. 253) and in other regions (e.g., Cordero et al. 2011). Structural differences between these datasets do not appear to significantly alter long-term temperature trends for the PNW. Regional mean temperature was correlated with global mean surface temperature on interannual

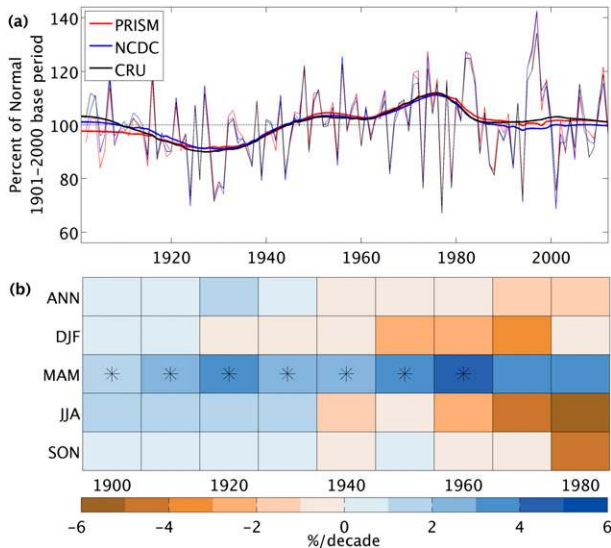


FIG. 2. As in Fig. 1, but for water year and seasonal precipitation percent of 1901–2000 normals and trends reported in percent per decade.

( $r^2 = 0.25$ ) and decadal (e.g., 1901–10,  $r^2 = 0.6$ ) time scales.

Warming trends were found in every season and time period except for spring 1980–2012, although statistically significant increases were observed in less than half of the time periods considered. The negative, albeit nonsignificant, temperature trend in spring from 1980 to 2012 is a consequence of several cool springs from 2008 to 2011 following a prolonged period of warm springs in the mid-1980s to mid-1990s, the latter of which was partially a result of low-frequency climate variability (Abatzoglou and Redmond 2007). With the exception of spring, recent seasonal temperature trends (starting in 1970 or 1980) were over twice as large as those from 1901–2012.

Regional water year precipitation (Fig. 2a) was predominantly below the twentieth-century average prior to 1945 and primarily above since then. On the decadal scale, the 1920s and 1930s were warm and dry, and the 1990s were warm and wet. The predominance of dry years (and multidecadal drought in the 1920s to 1930s) before 1945 results in a positive trend for water-year precipitation starting in years before 1940, whereas linear trends estimated from 1940 onward are negative (Fig. 2b). However, trends in water-year precipitation were not significant for any time periods considered. The quasi-decadal fluctuations in water-year precipitation are reflected in seasonal precipitation trends, which aside from spring were not statistically significant and rather varied (Fig. 2b). By contrast, spring precipitation exhibited positive trends over all time periods

considered, including statistically significant increases of approximately  $2\%–5\%$  decade $^{-1}$  for time periods starting in 1901 through 1960 and ending in 2012. It should be noted that average spring precipitation during the last 4 yr in the observational record (2009–12) was more than 30% above twentieth-century normals. Excluding these years from the trend analysis results in a moderated, but still significant, long-term increase over the period of record.

### b. Individual stations

Linear trends of maximum and minimum seasonal temperature for individual stations (1920–2012) elucidate the widespread nature of observed changes corroborating regional trends (Fig. 3). Although station trends were not spatially uniform, statistically significant increases in annual mean temperature were observed in a large majority of stations for trends for time periods commencing from 1940 to 1970 for maximum temperature and all time periods except 1980–2012 for minimum temperature, with additional heterogeneity in seasonal trends (Fig. 4). By contrast, typically only 5%–15% of stations had negative trends irrespective of starting period, reiterating the results of Mote (2003). Similar to previous global and regional studies, minimum temperatures increased more than maximum temperature from 1920 to 2012, whereas increases in maximum and minimum temperature were comparable for the last half century (e.g., Vose et al. 2005; Cordero et al. 2011).

Many stations showed a significant long-term decrease in diurnal temperature range (DTR), most notably in spring and summer (Figs. 3, 4). However, modest increases in station-averaged DTR were noted for 1970–2012 and 1980–2012 in both summer and autumn concurrent with decreased precipitation during these seasons. Diurnal temperature range during JJA and SON was moderately negatively correlated to seasonal precipitation (median correlation  $r = -0.41$  and  $r = -0.54$  in JJA and SON, respectively). This covariability between DTR and precipitation likely arises through dynamical (e.g., midlatitude quasi-stationary waves) and thermodynamic mechanisms (e.g., cloud cover and soil moisture).

Statistically significant positive trends in maximum and minimum temperature were observed in 35% and 45% of all stations and time periods considered, respectively. With the exception of spring, trends estimated for the most recent two time periods (i.e., 1970–2012, 1980–2012) were typically the largest of any time span considered with more than  $0.3^{\circ}\text{C decade}^{-1}$  warming observed for seasonal mean maximum temperature in summer and autumn from 1980 to 2012. Spring 1980–2012 was the only season that showed regionally



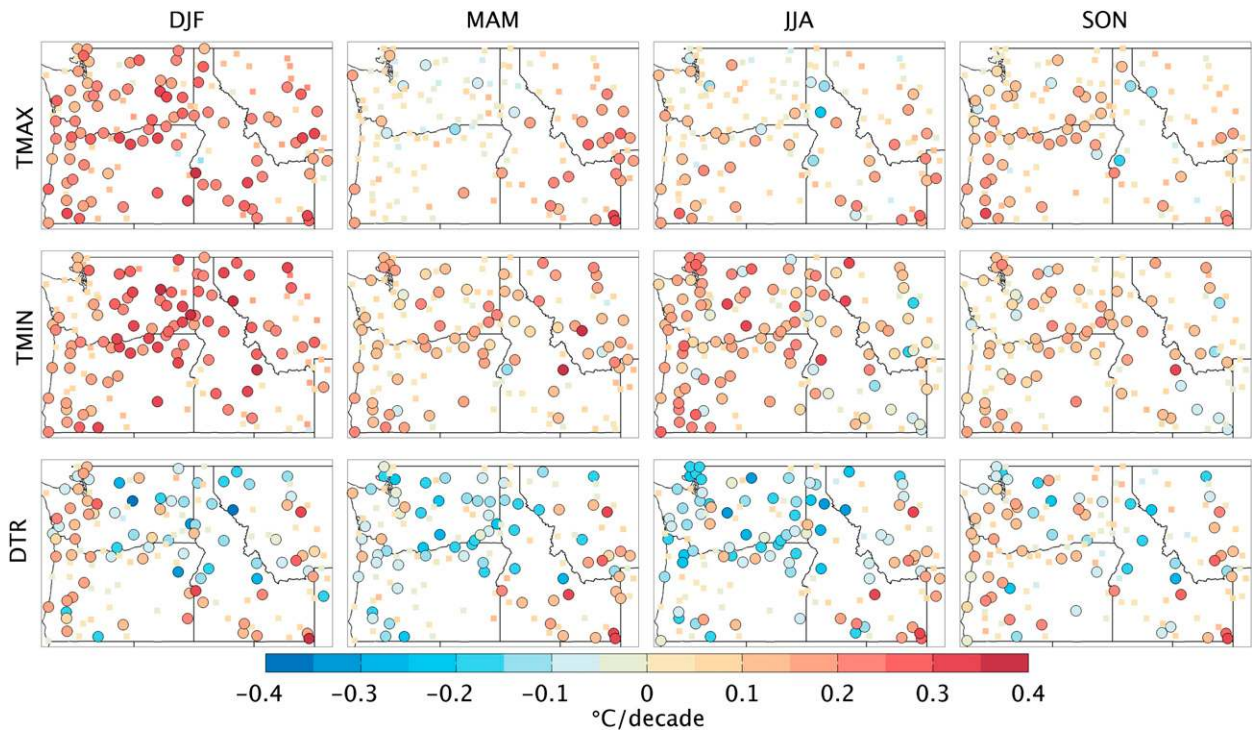


FIG. 3. Summary of station linear trends ( $^{\circ}\text{C decade}^{-1}$ ) in (top) maximum, (middle) minimum, and (bottom) diurnal temperature range for (from left to right) winter (DJF), spring (MAM), summer (JJA), and autumn (SON) for the period 1920–2012. Significant ( $p < 0.05$ ) trends are denoted by the large circles; trends that were not significant are denoted by smaller squares.

averaged cooling over any time period; this is seen both in the regionally averaged trends (Fig. 1) and in the fraction of stations with significant cooling versus those with significant warming.

Trends in precipitation were more heterogeneous in space and time (Fig. 5). Approximately 28% (5%) of stations observed significant increases (decreases) in water-year precipitation from 1920 to 2012, whereas approximately 1% (11%) of stations observed increases (decreases) in precipitation from 1980 to 2012. The overall paucity of stations reporting statistically significant trends in either direction for time periods commencing in 1940 or later suggest that interannual-to-decadal variability in precipitation (see also Fig. 2) exceeds any longer-term signal; this result is broadly consistent with other studies showing mixed trends in precipitation at similar latitudes (e.g., Groisman et al. 2004; Zhang et al. 2007). Trends in seasonal precipitation were generally varied, with less than 20% of stations in any given season exhibiting significant trends of the same sign. The primary exception was spring when positive trends of  $2\%–3\%$  decade $^{-1}$  were seen across many of the stations and for most periods of analysis.

An analogous examination of trends in the absolute maximum temperature per calendar year and absolute minimum temperature per water year is shown in Fig. 6.

Trends for the absolute maximum temperature were comparable in magnitude to annual mean maximum temperature for periods from 1950 onward, but are heterogeneous, similar to trends in annual absolute maxima observed globally (e.g., Karl et al. 1991). By contrast, trends in absolute minimum temperature exhibited strong positive trends, including in excess of  $1^{\circ}\text{C decade}^{-1}$  for 1970–2012 and 1980–2012. Increases in absolute minimum temperature are consistent with updated U.S. Department of Agriculture Plant Hardiness Zone Maps (Daly et al. 2012). While not explicitly examined in this study, Bumbaco et al. (2013) found that the frequency of nighttime minimum temperatures exceeding the 99th percentile for June–September increased substantially in western Washington and Oregon since 1901, whereas trends in the frequency of maximum temperatures exceeding the 99th percentile were not apparent.

Linear trends in the dates of the last spring freeze, first autumn freeze, and length of the freeze-free season provide additional support of pervasive warming across the PNW (Fig. 6). The date of the last spring freeze has advanced by, on average, 9 days since 1950, while the date of the first autumn freeze has been delayed by a comparable number of days since 1950. Collectively, these changes have resulted in an extension of the freeze-free

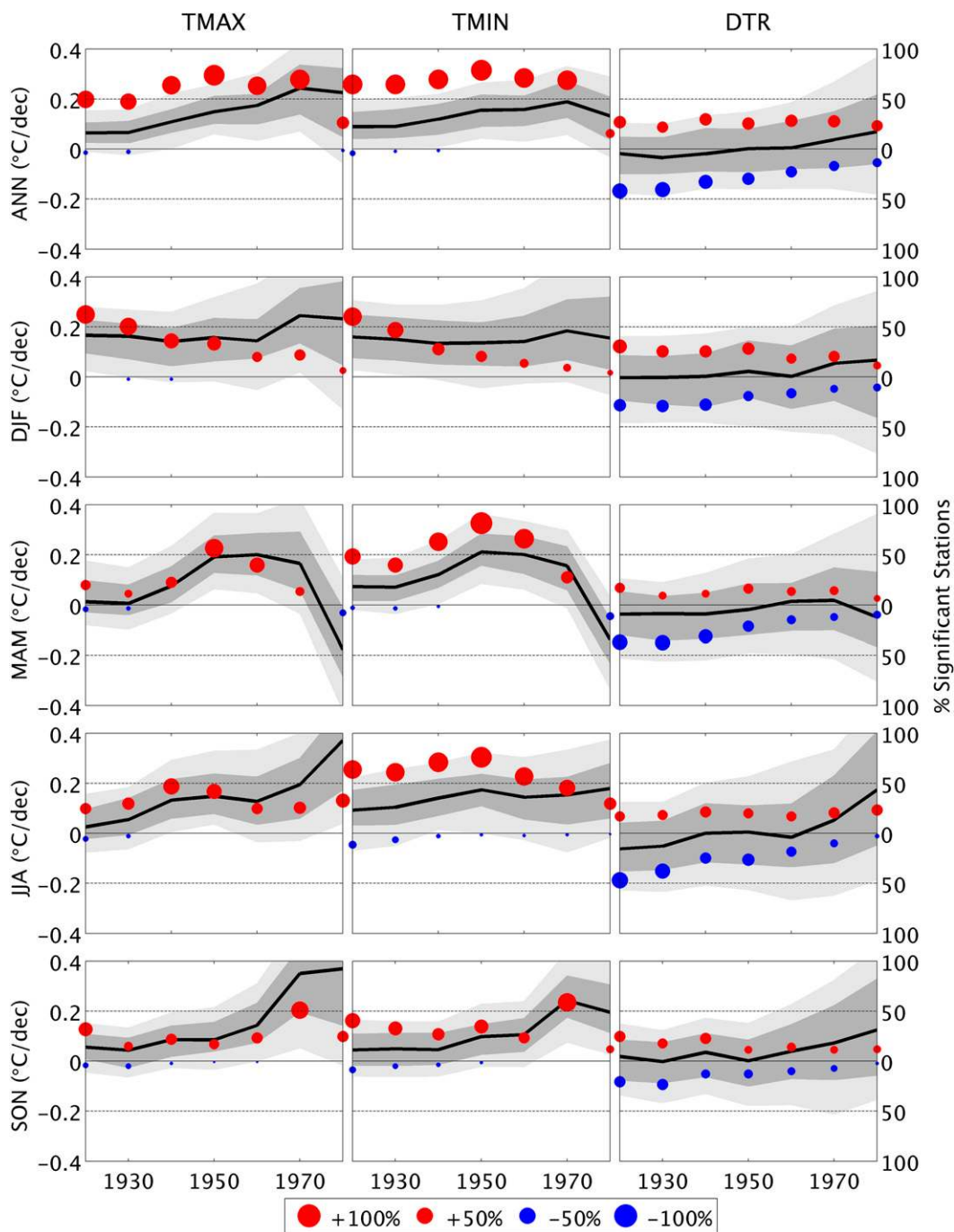


FIG. 4. Regional summary of the distribution of linear trends of maximum temperature, minimum temperature, and diurnal temperature range from 141 USHCN stations in the PNW. The  $x$  axis shows trends estimated for different periods of record ending in 2012 and beginning in 1920, incrementing every 10 yr through 1980. The light gray envelope encapsulates the 10th to 90th percentile of trends, the darker gray envelope shows the interquartile range, and the bold black line shows the median trend. The red and blue circles denote the percent of stations that observed significant positive and negative trends, respectively; both the area of the circle and its vertical displacement indicate this percentage.



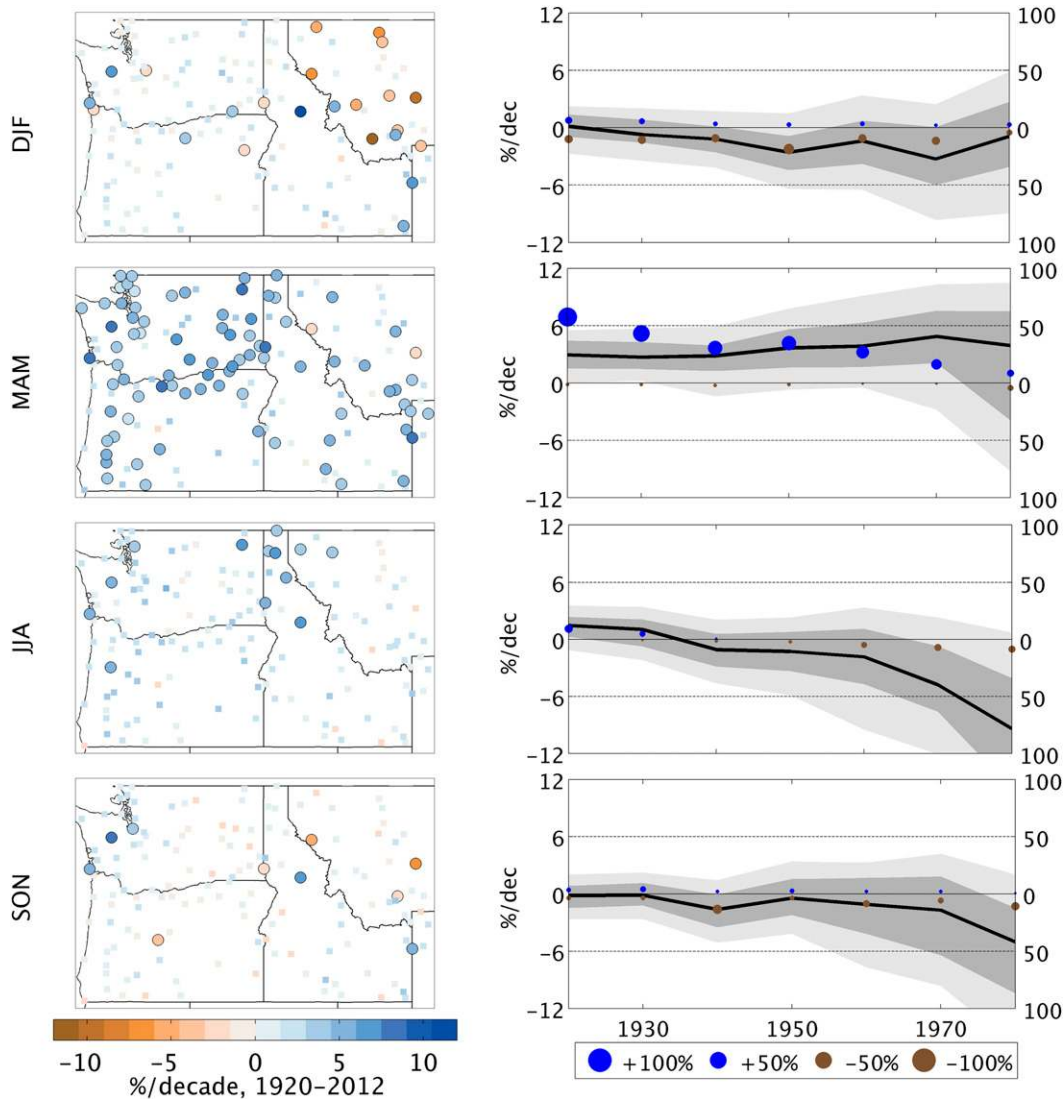


FIG. 5. (left) Summary of linear trends of seasonal precipitation (percent per decade) in (from top to bottom) winter (DJF), spring (MAM), summer (JJA), and autumn (SON) for the period 1920–2012. Significant ( $p < 0.05$ ) trends are denoted by the large circles; trends that were not significant are denoted by smaller squares. (right) As in Fig. 4, but for seasonal precipitation trends with brown and blue circles denoting the percent of stations that observed significant decreases and increases in precipitation, respectively.

season, or growing season by an average of approximately two weeks over the last four decades. Following trends in seasonal temperature, no significant changes in the date of the last spring freeze have been observed from 1980 to 2012, whereas there has been continued delay in the date of the first autumn freeze. These results are similar to analyses by Pederson et al. (2010), who reported significant increases in the number of days per year above freezing in western Montana.

Growing-season (freeze-free season) ETo exhibited a significant positive trend across multiple temporal

windows with a median trend of  $7\text{--}13 \text{ mm decade}^{-1}$  for time periods from 1950 onward (Fig. 7). This increase was associated with both an increase in the growing-season length, as depicted in Fig. 6, and increased vapor pressure deficit from July to September. Despite no long-term change in climatic water deficit for time periods commencing in the 1920s and 1930s (Dobrowski et al. 2013), declines in summer and autumn precipitation concomitant with increased summer ETo resulted in increased deficit in over 90% of all reporting stations and a regional median trend of about  $20 \text{ mm decade}^{-1}$  from 1980 to 2012.

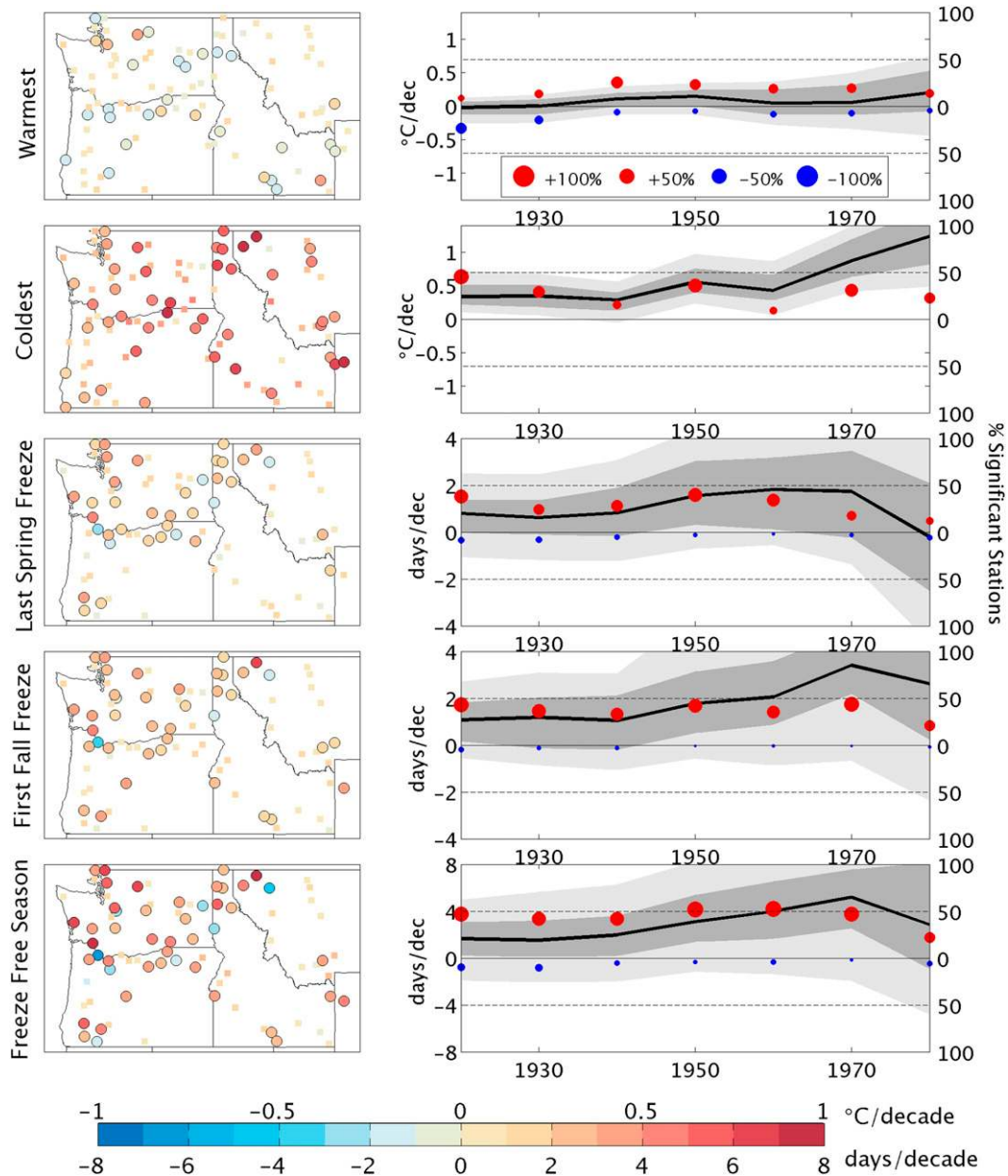


FIG. 6. (left) Summary of linear trends in (from top to bottom) annual absolute maximum temperature, winter absolute minimum temperature, last date prior to 1 July with minimum temperatures  $\leq 0^{\circ}\text{C}$ , first date after 1 July with minimum temperatures  $\leq 0^{\circ}\text{C}$ , and the length of the freeze-free season from 1920 to 2012. Significant ( $p < 0.05$ ) trends are denoted by the large circles; trends that were not significant are denoted by smaller squares. Warm colors denote an advancement, delay, and extension of the last spring freeze, first autumn freeze and freeze-free season, respectively. The color scale for the freeze-free season length has been multiplied by two. (right) As in Fig. 4, but for the respective set of indicators mentioned and shown on the left-hand panel.

*c. Multiple linear regression*

MLR models explained between 22% and 54% of the interannual variance in seasonal temperature (Table 1). Pearson correlation coefficients between seasonal temperature and the five different forcings

illustrate the strong relationships between seasonal temperature and internal climate variability manifested through ENSO and PNAr and weaker relationships to solar variability and volcanic aerosols (Fig. 8). Correlations to anthropogenic forcing were significant at  $p < 0.05$  for all seasons except autumn,

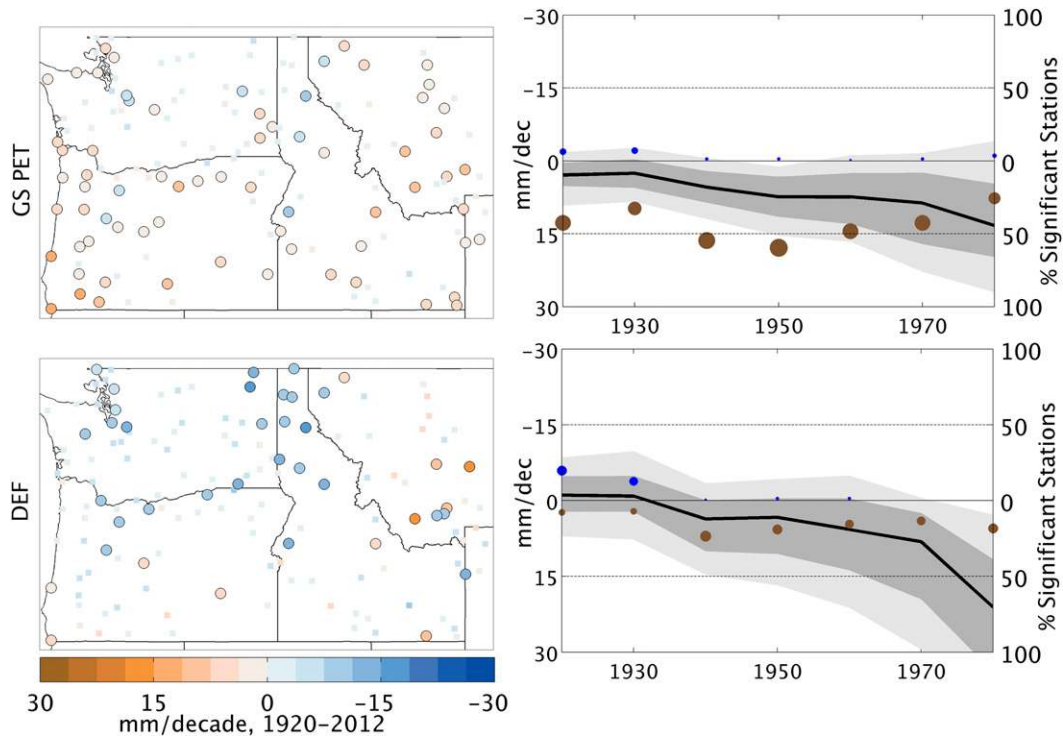


FIG. 7. As in Fig. 6, but for growing-season potential evapotranspiration (PET) and annual climatic water deficit. Note that brown colors represent increased PET and climatic water deficit.

as expected given the overall lower observed trend for autumn.

Corresponding linear regressions to internal climate variability (combined ENSO and PNA), volcanic, solar, and anthropogenic forcing over the 1901–2012 time period illustrate the magnitude of variability in seasonal temperature linearly imposed through these factors (Fig. 8). Internal climate variability was most pronounced during DJF with interannual contributions up to  $2.5^{\circ}\text{C}$ , less pronounced in MAM and SON and least in JJA. Solar and volcanic forcing were not significant contributors, except solar forcing during DJF and JJA that featured regional temperature variations of  $\sim 0.3^{\circ}\text{C}$  ( $p < 0.1$ ). The large error bars associated with volcanic aerosols were a consequence of a limited sample size of significant volcanic forcing events, restricting any statistical conclusions on the role of volcanic aerosols on regional temperature. Regressions to anthropogenic forcing showed a long-term warming trend of approximately  $0.45^{\circ}\text{C}$ – $0.75^{\circ}\text{C}$  over the 112-yr period of record, mostly since 1960.

Estimated linear trends in seasonal temperatures associated with the forcings are shown in Fig. 9 for three time periods. Long-term increases in temperature of around  $0.04^{\circ}\text{C}$ – $0.07^{\circ}\text{C}$  decade $^{-1}$  were primarily associated with anthropogenic forcing, as shown by the fact that the

residual after excluding all natural and anthropogenic forcings are, in general, statistically different from zero and similar to the observed trends, and the trends modulated on multidecadal time scales by internal variability and, to a lesser extent, solar variability (Table 1). The influence of internal variability contributed more substantially to multidecadal trends, including time periods

TABLE 1. Seasonal PNW temperature trends for 1901–2012,  $R^2$  of multiple linear regression, and regression coefficients. Values shown represent the median of the 1000 MLR models developed for each of the three observational datasets. Statistical significance at  $p < 0.1$  and  $p < 0.05$  is denoted when MLR models had the same sign for 90% and 95% of the models, respectively. Trends from observations were computed using the average anomalies from the three observational datasets. Values were rounded to the nearest hundredth. Obs is observation, Anthro is anthropogenic forcing, and Internal is combined MEI and PNAr.

Season	Trend ( $^{\circ}\text{C}$ decade $^{-1}$ )					$R^2$
	Obs	Anthro	Internal	Volcano	Solar	
DJF	0.12**	0.07**	0.02**	0	0.02*	0.45
MAM	0.04*	0.04*	0.02**	0	0	0.40
JJA	0.07**	0.06**	0	0	0.01*	0.24
SON	0.02*	0.04**	$-0.01^{**}$	0	0	0.54

\*  $p < 0.10$ .

\*\*  $p < 0.05$ .

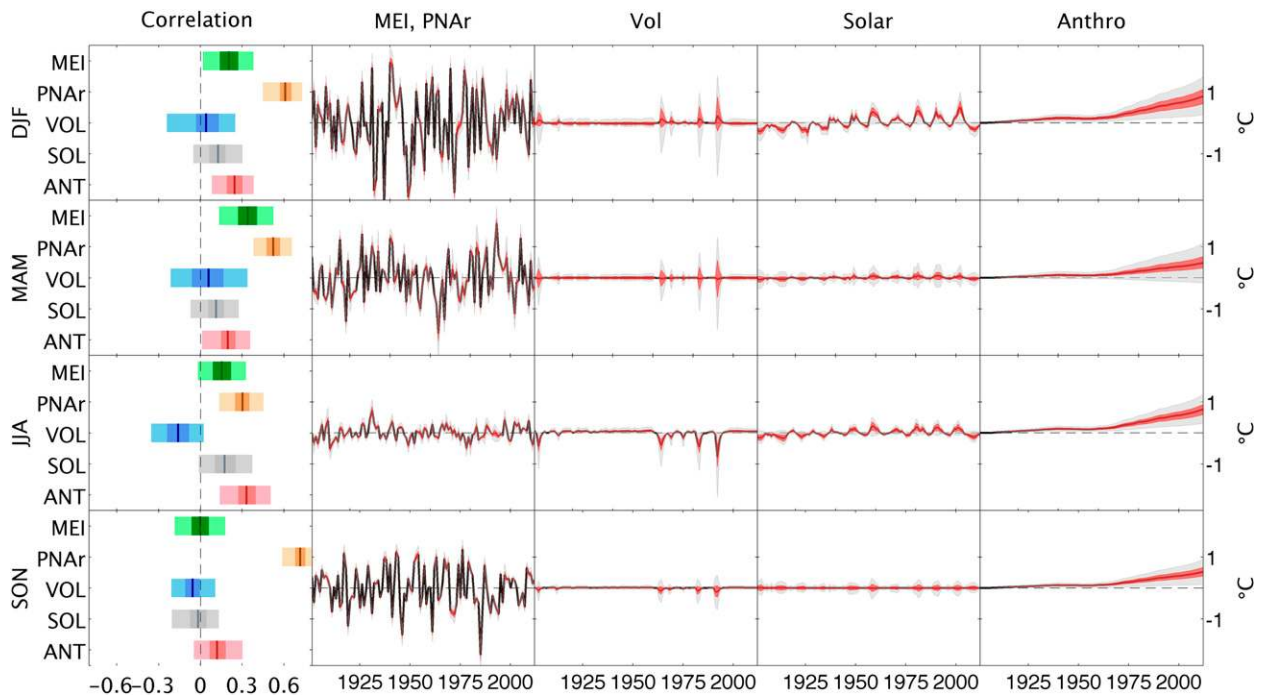


FIG. 8. (left column) Pearson's correlation coefficient between seasonal temperature for the five factors considered. The boxplots show the 95% confidence interval, interquartile range, and median of bootstrapped correlations by the light shading, dark shading, and solid line, respectively. (right four columns) Reconstructed contribution to seasonal temperature from the MLR for individual factors. The 95% confidence interval, interquartile range, and median of bootstrapped MLR contributions are denoted by the light gray shading, red shading, and black line, respectively. The combined influence of MEI and PNA is shown in the second column.

explicitly shown commencing in 1950 and 1980. For example, low-frequency variability in ENSO and PNAr compounded anthropogenic warming during DJF and MAM from 1950 to 2012 by up to an additional  $0.1^{\circ}\text{C decade}^{-1}$  and, conversely, ameliorated regional warming in MAM from 1980 to 2012 by  $0.2^{\circ}\text{C decade}^{-1}$ , largely explaining the negative trend in that season shown in Fig. 1. Trends in the residuals upon removal of the linear contribution from natural forcings were positive and statistically indistinguishable from trends attributed to anthropogenic forcing in most seasonal combinations considered.

Relationships between predictors and regional temperature were generally consistent across the three datasets examined. The primary exception was the larger signal attributed to solar forcing using CRU. Overall, the long-term (1901–2012) linear trend in seasonal temperature contributed by solar forcing in the MLR was approximately  $0.005^{\circ}\text{C decade}^{-1}$  larger for CRU than for PRISM or NCDC. This stronger relationship is realized by the larger increase in CRU temperature during the first half of the twentieth century, coincident with increased solar forcing. Consequently, MLR models with CRU exhibit heightened sensitivity to solar forcing across all time periods considered.

Modeled MLR results for regional precipitation were substantially weaker than for temperature and explained between 5% and 13% of the interannual variance in seasonal precipitation (Table 2, Fig. 10). The MEI was negatively correlated to precipitation in both autumn and winter, consistent with results from prior work (e.g., Ropelewski and Halpert 1986). The PNAr was negatively correlated to autumn precipitation, and volcanic aerosol was positively correlated to summer precipitation. While the statistical relationship between volcanic aerosol and summer precipitation in the PNW was significant, mechanisms through which global volcanic aerosol loading influence summer precipitation in the PNW are lacking. Correlations to anthropogenic forcing were only significant for spring, consistent with the observed positive trend in spring precipitation over the period of record.

Estimated linear trends in seasonal precipitation associated with the forcings are shown in Fig. 11 for three time periods. Anthropogenic contributions were not statistically distinguishable from zero for any of the time periods except in spring for all three time periods. The relationship between anthropogenic forcing and spring precipitation is of the same sign as the modeled response of anthropogenic forcing on both winter and spring, as



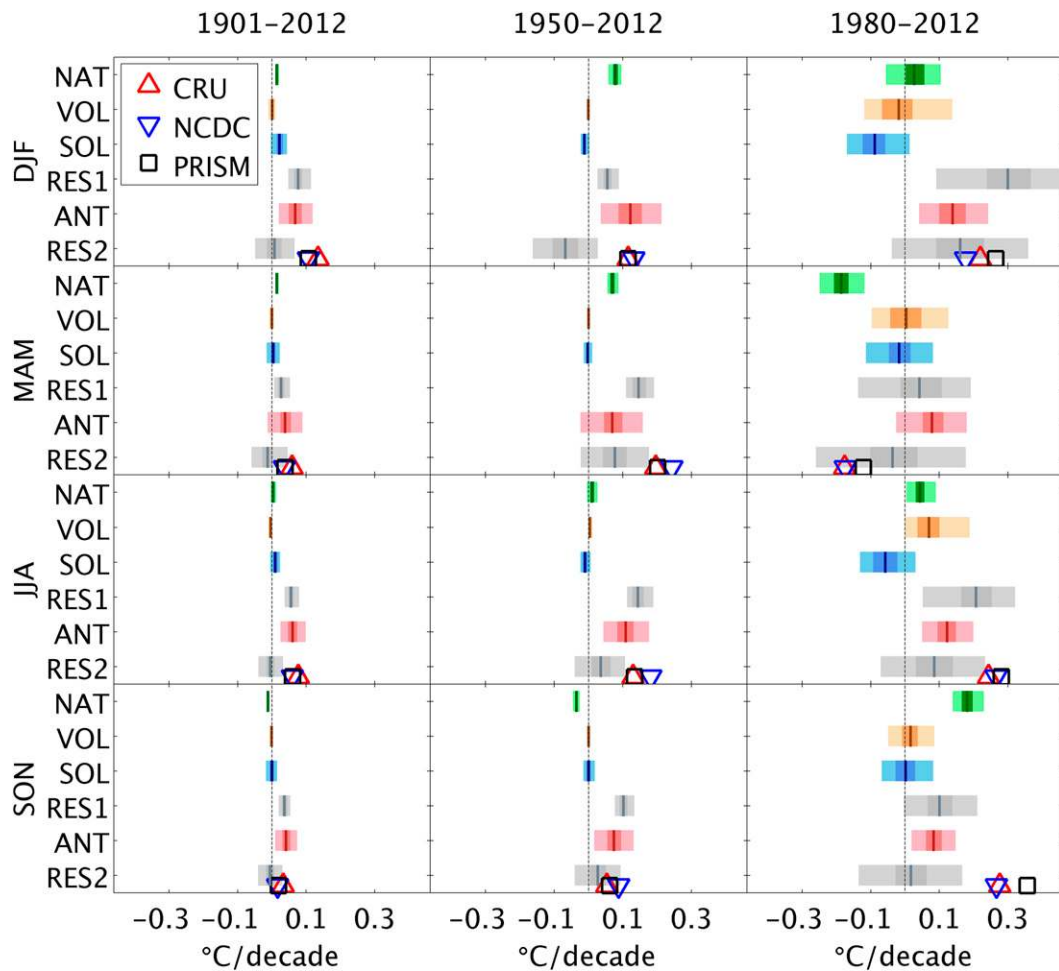


FIG. 9. Linear trend contribution of seasonal temperature ( $^{\circ}\text{C decade}^{-1}$ ) from internal variability of MEI and PNA (NAT), volcanic aerosols (VOL), solar forcing (SOL), residual after excluding all natural contributions (RES1), anthropogenic forcing (ANT), and residual after excluding natural and anthropogenic contributions (RES2) for three time spans: 1901–2012, 1950–2012, and 1980–2012. The boxplots show the 95% confidence interval, interquartile range, and median of bootstrapped linear trend by the light shading, dark shading, and solid line, respectively. Linear trends estimated from the three observational data are represented by symbols near the bottom of the plot.

realized through 27 models contributing to phase 5 of the CMIP (CMIP5). The models project an average 12% increase in regional December–May precipitation for 2071–2100 under the Representative Concentration Pathway 8.5 experiment compared to twentieth-century runs over the last half of the twentieth century, with increases noted in 25 of the 27 models. However, in simulations of the twentieth century, no significant trends in spring precipitation were found using a broader set of 41 CMIP5 climate models (95% confidence interval of the mean:  $-0.7\%$  to  $+1.2\%$   $\text{decade}^{-1}$ , Rupp et al. 2013). We reran the MLR models by excluding the first 50 years of record that included the multidecadal drought of the 1920s and 1930s. Results (not shown) failed to identify any significant signal attributable to anthropogenic forcing in

any season. Conversely, MLR models for temperature run over the same time period further strengthened relationships between anthropogenic forcing and seasonal temperature increase. The overall poor model skill

TABLE 2. As in Table 1, but for precipitation trends.

Season	Trend ( $\% \text{decade}^{-1}$ )					$R^2$
	Obs	Anthro	Internal	Volcano	Solar	
DJF	0.2	-0.2	-0.1*	0	0.2	0.05
MAM	1.8**	2.0**	0	0	0	0.09
JJA	1.3	0.4	0.2	0.3**	-0.1	0.13
SON	0	-0.1	0	0	0.2	0.13

\*  $p < 0.10$ .

\*\*  $p < 0.05$ .



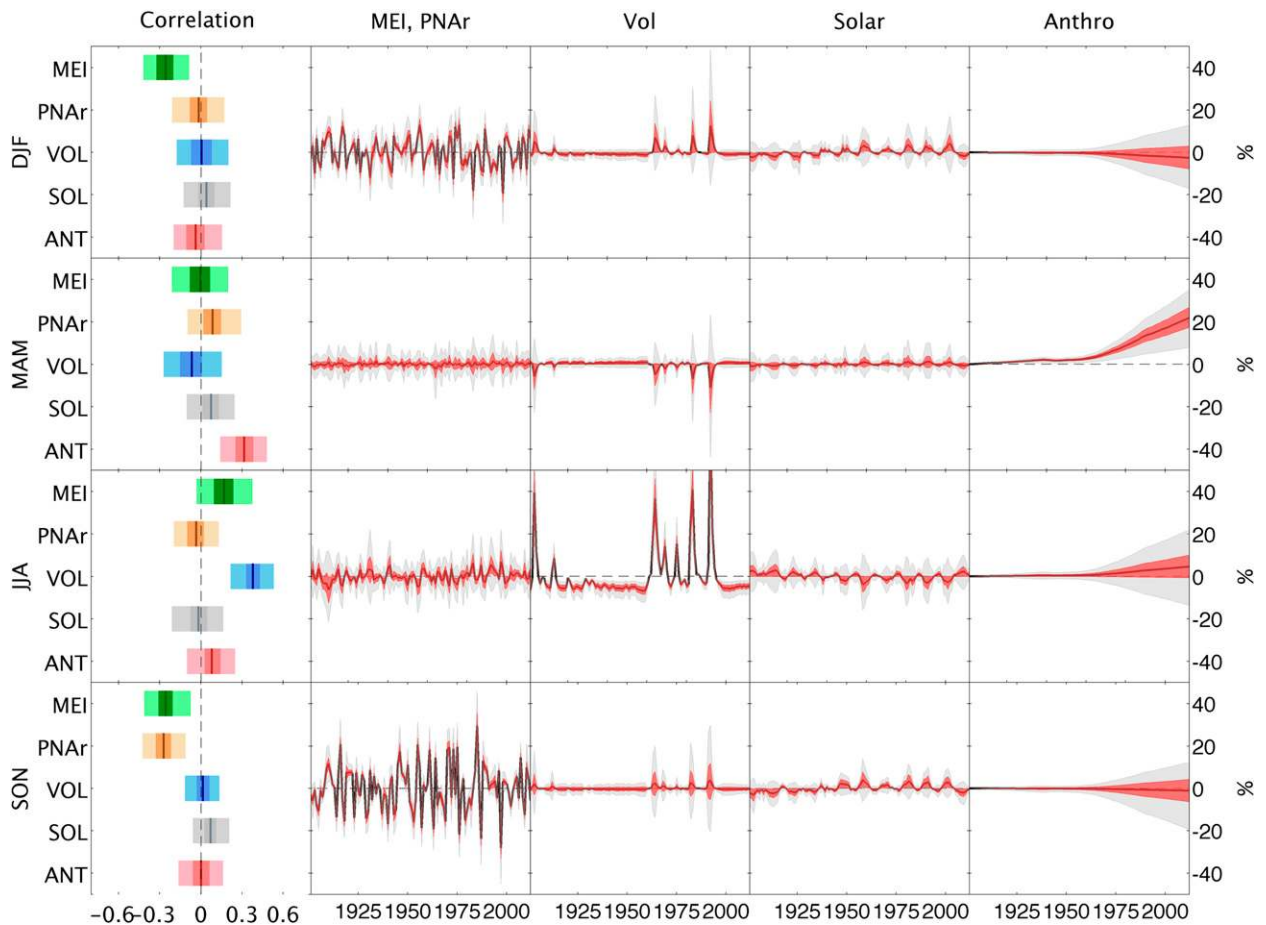


FIG. 10. As in Fig. 8, but for seasonal precipitation ( $\% \text{ decade}^{-1}$ ).

for regional precipitation suggests that additional facets of climate variability need to be considered in understanding sources of long-term precipitation changes.

Determining the true magnitude of the anthropogenic forcing on seasonal temperature and precipitation is complicated by the collinearity to other predictors over the entire period of record (Table 3). The long-term correlation of anthropogenic radiative forcing and solar variability is problematic for MLR. The result is that we cannot fully separate and isolate anthropogenic forcing using a linear regression approach. Moreover, MLR is a simple statistical approach that fails to account for the various physical processes. Two additional approaches were used to assess potential problems with our conclusions: (i) develop bootstrapped MLR using data only from 1951 to 2012 when solar variability and anthropogenic forcing were uncorrelated and (ii) develop bootstrapped MLR over the entire time period but exclude any resampled combination of years with collinearity between predictors ( $p < 0.05$ ). Our overall conclusions were robust to these additional experiments for MLR

temperature models. Likewise, different choices in the construction of predictors (e.g., using the operational MEI from 1950 to 2012 rather than just from 2006 to 2012) were found to weakly alter the relative influence of multidecadal trends attributable to natural variability over the past half century, but did not influence the overall conclusions of our study.

#### 4. Conclusions

Widespread seasonal warming trends from the early twentieth century through present have been observed in the Pacific Northwest of the United States and are further reflected by a longer freeze-free season and increased temperature of the coldest night each winter. More generally, we document a history of changes in regional temperature during the twentieth century similar to that seen globally, including rapid warming in the 1980s and 1990s and ambiguous short-term trends since 2000 linked to internal variability in the tropical Pacific (e.g., Lean and Rind 2009; Easterling and Wehner

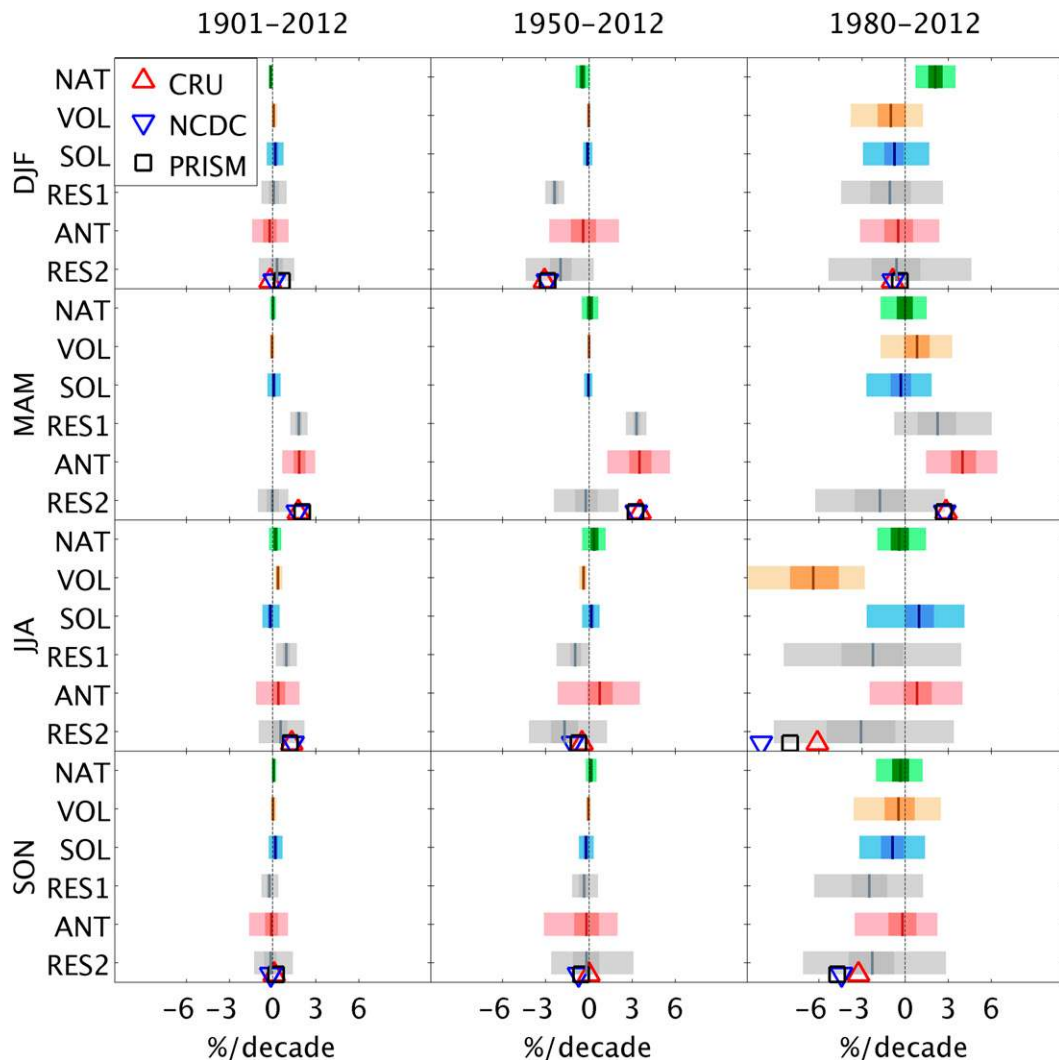


FIG. 11. As in Fig. 9, but for seasonal precipitation ( $\% \text{ decade}^{-1}$ ).

2009; Kosaka and Xie 2013). Seasonal temperature trends exhibited long-term warming with multidecadal variability, with the sole exception being nonsignificant cooling during spring from 1980 to 2012. Despite long-term decreases in diurnal temperature range (1920–2012), maximum and minimum temperatures increased at similar rates since 1950, similar to results noted earlier for the globe (Vose et al. 2005). Trends in seasonal precipitation were more heterogeneous, particularly for time periods commencing after the multidecadal drought in the 1920s and 1930s. However, longer growing seasons have increased ETo across the region and resulted in increased climatic water deficits over the past four decades.

A variety of global and regional forcings have influenced the evolution of seasonal temperature and precipitation in the PNW over the past century, as demonstrated through our MLR analysis. Anthropogenic forcing, primarily from

documented changes in well-mixed greenhouse gases, contributed to regional warming across all seasons at comparable rates ( $0.035^{\circ}\text{--}0.07^{\circ}\text{C decade}^{-1}$  from 1901 to 2012). Furthermore, the two leading modes of internal climate variability pertinent to the region, namely, ENSO and PNA, reinforced or counteracted effects of anthropogenic forcing on seasonal temperature trends at multidecadal time scales. Most notably, ENSO and the PNA appear to have hastened the pace of regional warming during DJF and MAM since the mid-twentieth century while buffering warming during SON (e.g., Abatzoglou and Redmond 2007). By contrast, natural variability contributed to the recent (1980–2012) cooling during MAM and masked anthropogenic regional warming similar to that seen on global scales over short ( $<20$  yr) time periods (Foster and Rahmstorf 2011). Solar variability and volcanic aerosols did not exhibit

TABLE 3. Average Pearson correlation coefficients for predictor variables by season for the period 1901–2012 calculated from bootstrapped data. Statistical significance is denoted at  $p < 0.1$  and  $p < 0.05$  by one and two asterisks, respectively.

	MEI	PNAr	Volcano	Solar	Anthro
DJF					
PNAr	0.00	1			
Volcano	0.26**	−0.07	1		
Solar	0.05	−0.07	0.04	1	
Anthro	0.08	0.08	0.08	0.24**	1
MAM					
PNAr	0.00	1			
Volcano	0.28*	−0.09	1		
Solar	0.12*	0.05	0.07	1	
Anthro	0.07	0.14*	0.05	0.2**	1
JJA					
PNAr	0.00	1			
Volcano	0.21*	−0.12**	1		
Solar	0.13*	−0.03	0.03	1	
Anthro	0.22**	0.04	0.05	0.15*	1
SON					
PNAr	0.00	1			
Volcano	0.14*	−0.06	1		
Solar	0.01	−0.08	0.07	1	
Anthro	0.07	−0.09	0.07	0.17**	1

a statistically significant signal on regional temperature trends over the period of record. The residuals of seasonal temperature upon removing the linear influences of natural forcings showed consistent warming trends across the four seasons. The temperature trends in the residuals are within the confidence interval of trends associated with anthropogenic forcing and modeled temperature trends averaged over the region from 41 CMIP5 climate models run using twentieth-century forcings (95% confidence interval of the mean  $+0.035^{\circ}$  to  $+0.092^{\circ}\text{C decade}^{-1}$ , Rupp et al. 2013). These results suggest that regional warming is consistent with anthropogenic radiative forcing and inconsistent with other factors considered in this study and similar to the findings of related studies (e.g., Wang et al. 2009).

Compared to the analysis of Lean and Rind (2008), in which these predictors explained 75% of mean annual global temperature variability using MLR, our analysis explained only 24%–54% of the interannual variance in regional temperature variability, likely an attribute of disaggregation to regional and seasonal time scales. At the decadal time scale, MLR models explained between 58% and 78% of variability in observed seasonal temperature. Additional forcings that were not considered include (i) large-scale modes of climate variability aside from ENSO and PNA, (ii) regional land-use change, and

(iii) land surface feedbacks associated with snow cover or soil moisture anomalies. The Pacific decadal oscillation (PDO) has often been implicated in PNW climate variability. We did not include the PDO as a separate predictor in the results presented here because Newman (2007) showed the PDO to be a low-frequency mid-latitude response of ENSO that is not statistically independent from ENSO. To further test this hypothesis we reran the MLR analysis by including the PDO residual (after excluding the influence of MEI and PNA) in addition to MEI and PNAr. The conclusions of our study were largely unchanged: MLR models that included the PDO had seasonal temperature trends over the periods considered that were generally within  $0.01^{\circ}\text{C decade}^{-1}$  of models that did not include the PDO.

Structural uncertainty in regional datasets did not alter the main conclusions of our analysis. The use of varied datasets and the introduction of bootstrap resampling help provide confidence intervals in our MLR model. However, the use of a simple linear model overlooks any nonlinear interactions among forcings and assumes a stationary influence through time. That is, this approach falters if, for example, changes in the character of ENSO are a consequence of rising greenhouse gases. Of the remaining unexplained variance, we find negative correlations between the residual of temperature and regional precipitation during MAM ( $r = -0.45$ ) and JJA ( $r = -0.52$ ) when MLR accounts for the least amount of variance explained. This covariability between regional temperature and precipitation occurs during the two seasons when solar radiation is highest, consistent with thermodynamic relationships that link precipitation and temperature (increased cloud cover, snow cover, and soil moisture) in addition to larger-scale synoptic patterns that dynamically couple temperature and precipitation. The weaker attribution of increases in spring temperature to anthropogenic forcing over the 1901–2012 period ( $p < 0.1$ ) may be partially due to the coincident long-term increase in spring precipitation.

Regional precipitation trends were varied and exhibited multidecadal variability weakly explained by the forcings considered. Long-term increases in spring precipitation are generally consistent with climate modeling results. However, the magnitude of change attributed to anthropogenic forcing in our exercise appears significantly larger than CMIP5 model projections to anthropogenic forcing experiments over the twenty-first century. Furthermore, we find that MLR results for regional precipitation were not robust to different time periods considered and highlight the need for additional facets of natural climate variability not considered in our analysis to resolve this discrepancy (e.g., Hoerling et al. 2010).

Climate variability has played and will continue to play a significant role in the pace of climate change at regional and seasonal scales. There remains significant uncertainty concerning the role of anthropogenic forcing on climate variability and their teleconnections (e.g., Stevenson 2012). Irrespective of anthropogenically forced changes in large-scale climate modes, internal climate variability is expected to be a prime contributor to uncertainty in near-term climate projections at regional scales for the next several decades by exacerbating or ameliorating anthropogenic forcing (e.g., Hawkins and Sutton 2011), particularly in areas like the Pacific Northwest (Deser et al. 2012).

*Acknowledgments.* We are appreciative of constructive feedback from John Nielsen-Gammon, and an anonymous reviewer who helped improve the quality of our manuscript. This research was funded by the U.S. Department of Agriculture National Institute for Food and Agriculture Award 2011-68002-30191, U.S. Department of the Interior via the Northwest Climate Science Center Award G12AC20495, and NOAA Regional Integrated Science Assessment (RISA) program Grant NA10OAR4310218.

## APPENDIX

### Variables Used in Multiple Linear Regression

To represent ENSO, we investigated several approaches and then selected the extended Multivariate El Niño Index (MEI) from 1900 to 2005 (Wolter and Timlin 2011) and the operational MEI from 2006 to 2012. A linear model of the extended MEI using the operational MEI over the period of common data (1950–2005) was used to adjust the post-2005 data for consistency across datasets. The monthly PNA index was calculated using the modified pointwise method (Wallace and Gutzler 1981) using monthly detrended 500-hPa geopotential height anomalies (1871–2011) from twentieth-century reanalysis (Compo et al. 2011) and National Centers for Environmental Prediction–National Center for Atmospheric Research (NCEP–NCAR) Reanalysis 1 from 1948 to 2012. A linear model of the PNA derived from the twentieth-century reanalysis using the PNA derived from NCEP–NCAR Reanalysis 1 (1948–2012) over the period of common data (1948–2011) was used to adjust monthly PNA indices for 2012. We chose to detrend 500-hPa height anomalies prior to calculating the PNA index given its similarity to the cold ocean–warm land pattern (Wallace et al. 1995) in the Pacific–North American sector that projects onto an anthropogenic forcing response (Broccoli et al. 1998).

It is unclear to what extent exogenous forcing has influenced internal climate variability. However, given the interest in avoiding collinearity in predictors and challenges in separating radiative versus dynamical changes in natural climate variability, our choice to detrend data prior to MLR is consistent with prior studies (Thompson et al. 2009).

Annual mean total solar irradiance (TSI) for 1901–2012 from Wang et al. (2005) ([http://lasp.colorado.edu/lisird/tsi/historical\\_tsi.html](http://lasp.colorado.edu/lisird/tsi/historical_tsi.html), downloaded 2 August 2013) was augmented with Physikalisch-Meteorologisches Observatorium Davos (PMOD) TSI composite from 1978 to 2012. We chose to use the PMOD composite over the contemporary time period as it better adheres to observed sunspot numbers over the past two decades and the minima in solar activity during solar cycle 23 relative to complementary TSI estimates (Frohlich 2012). A linear model of TSI using PMOD data over the period of common data (1978–2012) was used to adjust PMOD estimates from 1978 to 2012 to the longer term TSI data. TSI data from Wang et al. (2005) were used from 1901 to 1977. Volcanic aerosols were represented by monthly-mean optical thickness of global stratospheric aerosols provided by the NASA Goddard Institute for Space Sciences (<http://data.giss.nasa.gov/modelforce/strataer/>, downloaded 2 August 2013). Historical total anthropogenic radiative forcings used in the representative concentration pathway (RCP) datasets of Meinshausen et al. (2011) were used from 1900 to 2005 and represent the sum of radiative forcing by well-mixed greenhouse gases, ozone, tropospheric aerosols, and land use and snow albedo changes. Anthropogenic radiative forcing from RCP6.0 was used in the absence of directly comparable anthropogenic radiative forcing estimates from 2006 to 2012. Our results are largely unchanged using alternative RCP pathways from 2006 to 2012.

## REFERENCES

- Abatzoglou, J. T., 2011: Influence of the PNA on declining mountain snowpack in the Western United States. *Int. J. Climatol.*, **31**, 1135–1142, doi:10.1002/joc.2137.
- , and K. T. Redmond, 2007: Asymmetry between trends in spring and autumn temperature and circulation regimes over western North America. *Geophys. Res. Lett.*, **34**, L18808, doi:10.1029/2007GL030891.
- Alexander, L. P., and Coauthors, 2013: Summary for policymakers. *Climate Change 2013: The Physical Science Basis*, T. S. Stocker et al., Eds., Cambridge University Press, 1–27. [Available online at <http://www.ipcc.ch/>.]
- Allen, R. G., L. S. Pereira, D. Raes, and M. Smith, 1998: Crop evapotranspiration: Guidelines for computing crop water requirements. FAO Irrigation and Drainage Paper 56, Food and Agricultural Organization of the United Nations, Rome, Italy.

- 300 pp. [Available online at <http://www.fao.org/docrep/x0490e/x0490e00.htm>.]
- Betts, A. K., 2011: Vermont climate change indicators. *Wea. Climate Soc.*, **3**, 106–115.
- Broccoli, A. J., N.-C. Lau, and M. J. Nath, 1998: The cold ocean–warm land pattern: Model simulation and relevance to climate change detection. *J. Climate*, **11**, 2743–2763.
- Bonfils, C., and Coauthors, 2008: Detection and attribution of temperature changes in the mountainous western United States. *J. Climate*, **21**, 6404–6424.
- Bumbaco, K. A., K. D. Dello, and N. A. Bond, 2013: History of Pacific Northwest heat waves: Synoptic patterns and trends. *J. Appl. Meteor. Climatol.*, **52**, 1618–1631.
- Cohen, J. L., J. C. Furtado, M. Barlow, V. A. Alexeev, and J. E. Chery, 2012: Asymmetric seasonal temperature trends. *Geophys. Res. Lett.*, **39**, L04705, doi:10.1029/2011GL050582.
- Cordero, E. C., W. Kessomkiat, J. Abatzoglou, and S. A. Mauget, 2011: The identification of distinct patterns in California temperature trends. *Climatic Change*, **108**, 357–382.
- Compo, G. P., and Coauthors, 2011: The Twentieth Century Reanalysis Project. *Quart. J. Roy. Meteor. Soc.*, **137**, 1–28, doi:10.1002/qj.776.
- Daly, C., M. D. Halbleib, J. I. Smith, W. P. Gibson, M. K. Doggett, G. H. Taylor, J. Curtis, and P. A. Pasteris, 2008: Physiographically sensitive mapping of temperature and precipitation across the conterminous United States. *Int. J. Climatol.*, **28**, 2031–2064, doi:10.1002/joc.1688.
- , M. P. Widrlechner, M. D. Halbleib, J. I. Smith, and W. P. Gibson, 2012: Development of a new USDA Plant Hardiness Zone Map for the United States. *J. Appl. Meteor. Climatol.*, **51**, 242–264.
- Deser, C., R. Knutti, S. Solomon, and A. S. Phillips, 2012: Communication of the role of natural variability in future North American climate. *Nat. Climate Change*, **2**, 775–779, doi:10.1038/nclimate1562.
- Dobrowski, S. Z., J. Abatzoglou, A. K. Swanson, A. Mynsberge, J. A. Greenberg, Z. Holden, and M. K. Schwartz, 2013: The climate velocity of the contiguous United States during the 20th century. *Global Change Biol.*, **19**, 241–251, doi:10.1111/gcb.12026.
- Easterling, D. R., and M. F. Wehner, 2009: Is the climate warming or cooling? *Geophys. Res. Lett.*, **36**, L08706, doi:10.1029/2009GL037810.
- Foster, G., and S. Rahmstorf, 2011: Global temperature evolution 1979–2010. *Environ. Res. Lett.*, **6**, 044022, doi:10.1088/1748-9326/6/4/044022.
- Frohlich, C., 2012: Total solar irradiance observations. *Surv. Geophys.*, **33**, 453–473.
- Groisman, P. Y., R. W. Knight, T. R. Karl, D. R. Easterling, B. Sun, and J. H. Lawrimore, 2004: Contemporary changes of the hydrological cycle over the contiguous United States: Trends derived from in situ observations. *J. Hydrometeorol.*, **5**, 64–85.
- Hansen, J., and Coauthors, 2007: Climate simulations for 1880–2003 with GISS modelE. *Climate Dyn.*, **29**, 661–696, doi:10.1007/s00382-007-0255-8.
- Harris, I., P. D. Jones, T. J. Osborn, and D. H. Lister, 2013: Updated high-resolution grids of monthly climatic observations—The CRU TS3.10 dataset. *Int. J. Climatol.*, doi:10.1002/joc.3711, in press.
- Hawkins, E., and R. Sutton, 2011: The potential to narrow uncertainty in projections of regional precipitation change. *Climate Dyn.*, **37**, 407–418, doi:10.1007/s00382-010-0810-6.
- Hoerling, M., J. Eischeid, and J. Perlwitz, 2010: Regional precipitation trends: Distinguishing natural variability from anthropogenic forcing. *J. Climate*, **23**, 2131–2145.
- Horel, J. D., and J. M. Wallace, 1981: Planetary-scale atmospheric phenomena associated with the Southern Oscillation. *Mon. Wea. Rev.*, **109**, 813–829.
- Jensen, M. E., R. D. Burman, and R. G. Allen, Eds., 1990: Evapotranspiration and Irrigation Water Requirements. ASCE Manuals and Reports on Engineering Practices, No. 70, American Society for Civil Engineers, 360 pp.
- Karl, T. R., G. Kukla, V. N. Razuvayev, M. J. Changery, R. G. Quayle, R. R. Heim Jr., D. R. Easterling, and C. B. Fu, 1991: Global warming—Evidence for asymmetric diurnal temperature change. *Geophys. Res. Lett.*, **18**, 2253–2256.
- Kosaka, Y., and S.-P. Xie, 2013: Recent global-warming hiatus tied to equatorial Pacific surface cooling. *Nature*, **501**, 403–407, doi:10.1038/nature12534.
- Lean, J. L., and D. H. Rind, 2008: How natural and anthropogenic influences alter global and regional surface temperatures: 1889 to 2006. *Geophys. Res. Lett.*, **35**, L18701, doi:10.1029/2008GL034864.
- , and —, 2009: How will Earth’s surface temperature change in future decades? *Geophys. Res. Lett.*, **36**, L15708, doi:10.1029/2009GL038932.
- Liebmann, B., R. M. Dole, C. Jones, I. Bladé, and D. Allured, 2010: Influence of choice of time period on global surface temperature trend estimates. *Bull. Amer. Meteor. Soc.*, **91**, 1485–1491.
- McRoberts, D. B., and J. W. Nielsen-Gammon, 2011: A new homogenized climate division precipitation dataset for analysis of climate variability and climate change. *J. Appl. Meteor. Climatol.*, **50**, 1187–1199.
- Meinshausen, M., and Coauthors, 2011: The RCP greenhouse gas concentrations and their extension from 1765 to 2300. *Climatic Change*, **109**, 213–241, doi:10.1007/s10584-011-0156-z.
- Menne, M. J., C. N. Williams Jr., and R. S. Vose, 2009: The U.S. Historical Climatology Network monthly temperature data, version 2. *Bull. Amer. Meteor. Soc.*, **90**, 993–1007.
- Mitchell, K. E., and Coauthors, 2004: The multi-institution North American Land Data Assimilation System (NLDAS): Utilizing multiple GCIP products and partners in a continental distributed hydrological modeling system. *J. Geophys. Res.*, **109**, D07S90, doi:10.1029/2003JD003823.
- Morice, C. P., J. J. Kennedy, N. A. Rayner, and P. D. Jones, 2012: Quantifying uncertainties in global and regional temperature change using an ensemble of observational estimates: The HadCRUT4 data set. *J. Geophys. Res.*, **117**, D08101, doi:10.1029/2011JD017187.
- Mote, P. W., 2003: Trends in temperature and precipitation in the Pacific Northwest. *Northwest Sci.*, **77**, 271–282.
- , and E. P. Salathé Jr., 2010: Future climate in the Pacific Northwest. *Climatic Change*, **102**, 29–50, doi:10.1007/s10584-010-9848-z.
- , A. F. Hamlet, M. P. Clark, and D. P. Lettenmaier, 2005: Declining mountain snowpack in western North America. *Bull. Amer. Meteor. Soc.*, **86**, 39–49.
- Newman, M., 2007: Interannual to decadal predictability of tropical and North Pacific sea surface temperatures. *J. Climate*, **20**, 2333–2356.
- Pederson, G. T., L. J. Graumlich, D. B. Fagre, T. Kipfer, and C. Muhlfield, 2010: A century of climate and ecosystem change in Western Montana: What do recent temperature trends portend? A view from western Montana, USA. *Climatic Change*, **98**, 133–154, doi:10.1007/s10584-009-9642-y.



- Pierce, D. W., and Coauthors, 2008: Attribution of declining western U.S. snowpack to human effects. *J. Climate*, **21**, 6425–6444.
- Ropelewski, C. F., and M. S. Halpert, 1986: North American precipitation and temperature patterns associated with the El Niño/Southern Oscillation (ENSO). *Mon. Wea. Rev.*, **114**, 2352–2362.
- Rupp, D. E., J. T. Abatzoglou, K. C. Hegewisch, and P. W. Mote, 2013: Evaluation of CMIP5 20th century climate simulations for the Pacific Northwest USA. *J. Geophys. Res. Atmos.*, **118**, 10 884–10 906, doi:10.1002/jgrd.50843.
- Santer, B. D., T. M. L. Wigley, J. S. Boyle, D. J. Gaffen, J. J. Hnilo, D. Nychka, D. E. Parker, and K. E. Taylor, 2000: Statistical significance of trends and trend differences in layer-average atmospheric temperature time series. *J. Geophys. Res.*, **105** (D6), 7337–7356.
- Stevenson, S., 2012: Significant changes to ENSO strength and impacts in the twenty-first century: Results from CMIP5. *Geophys. Res. Lett.*, **39**, L17703, doi:10.1029/2012GL052759.
- Stott, P. A., N. P. Gillett, G. C. Hegerl, D. J. Karoly, D. A. Stone, X. Zhang, and F. Zwiers, 2010: Detection and attribution of climate change: A regional perspective. *Wiley Interdiscip. Rev.: Climate Change*, **1**, 192–211, doi:10.1002/wcc.34.
- Thompson, D. W. J., J. M. Wallace, P. D. Jones, and J. Kennedy, 2009: Identifying signatures of natural climate variability in time series of global-mean surface temperature: Methodology and insights. *J. Climate*, **22**, 6120–6141.
- Trenberth, K. E., and Coauthors, 2007: Observations: Surface and atmospheric climate change. *Climate Change 2007: The Physical Science Basis*, S. Solomon et al., Eds., Cambridge University Press, 235–336.
- Vose, R. S., D. R. Easterling, and B. Gleason, 2005: Maximum and minimum temperature trend for the globe: An update through 2004. *Geophys. Res. Lett.*, **32**, L23822, doi:10.1029/2005GL024379.
- Wallace, J. M., and D. S. Gutzler, 1981: Teleconnections in the geopotential height field during the Northern Hemisphere winter. *Mon. Wea. Rev.*, **109**, 784–812.
- , Y. Zhang, and J. A. Renwick, 1995: Dynamic contribution to hemispheric mean temperature trends. *Science*, **270**, 780–783.
- , Q. Fu, B. V. Smoliak, P. Lin, and C. M. Johanson, 2012: Simulated versus observed patterns of warming over the extratropical Northern Hemisphere continents during the cold season. *Proc. Natl. Acad. Sci. USA*, **109**, 14 337–14 342.
- Wang, H., S. Schubert, M. Suarez, J. Chen, M. Hoerling, A. Kumar, and P. Pegion, 2009: Attribution of the seasonality and regionality in climate trends over the United States during 1950–2000. *J. Climate*, **22**, 2571–2590.
- Wang, Y.-M., J. L. Lean, and N. R. Sheeley Jr., 2005: Modeling the Sun's magnetic field and irradiance since 1713. *Astrophys. J.*, **625**, 522–538.
- Willmott, C. J., C. M. Rowe, and Y. Mintz, 1985: Climatology of the terrestrial seasonal water cycle. *J. Climatol.*, **5**, 589–606.
- Wolter, K., and M. S. Timlin, 2011: El Niño/Southern Oscillation behaviour since 1871 as diagnosed in an extended multivariate ENSO index (MEI.ext). *Int. J. Climatol.*, **31**, 1074–1087, doi:10.1002/joc.2336.
- Zhang, X., F. W. Zwiers, G. C. Hegerl, F. H. Lambert, N. P. Gillett, S. Solomon, P. A. Stott, and T. Nozawa, 2007: Detection of human influence on twentieth-century precipitation trends. *Nature*, **448**, 461–465, doi:10.1038/nature06025.